

Microstructure and Properties of Cu-Fe-Cr-Ag Alloy Prepared by Directional Solidification and Upward Continuous Casting



DAWEI YUAN, JINSHUI CHEN, XIANGPENG XIAO, BAOJUN HAN, HAO HUANG, BAIXIONG LIU, and BIN YANG

A Cu-Fe-Cr-Ag alloy was prepared by directional solidification (DS) and upward continuous casting (UCC) to study the effect of different casting methods on the structure and properties of Cu-Fe-Cr-Ag. The results showed that the directionally solidified Cu-Fe-Cr-Ag alloy had excellent mechanical properties and conductivity. After cold drawing and isothermal aging, the peak tensile strength (789 MPa) and peak conductivity (65.5 pct IACS) of directionally solidified Cu-Fe-Cr-Ag alloy were 21 MPa and 4.7 pct IACS higher, respectively, than those that of the upward continuously casted Cu-Fe-Cr-Ag alloy. Compared to upward continuously casted Cu-Fe-Cr-Ag alloy, the Fe dendrites in directionally solidified Cu-Fe-Cr-Ag alloy were much finer, more uniform, and arranged along the direction of the magnetic field. Cu and Ag formed a Cu-Ag eutectic structure at the edge of the directionally solidified Cu-Fe-Cr-Ag alloy rod. After multi-stage thermomechanical treatment, Ag was mainly distributed around the material and formed a structure similar to Ag-clad Cu. The directionally solidified Cu-Fe-Cr-Ag alloy had a smaller lattice constant and finer Fe fibers. The small lattice constant and Fe fibers and the special distribution of Ag lead to the excellent comprehensive performance of the directionally solidified Cu-Fe-Cr-Ag alloy.

<https://doi.org/10.1007/s11661-021-06239-z>

© The Minerals, Metals & Materials Society and ASM International 2021

I. INTRODUCTION

OWING to its high strength and good conductivity, the Cu-Fe alloy has a wide range of application prospects in 5G mobile phones as well as in high-conductivity, high-tension wires, and welding wires. The Cu-Fe alloy undergoes liquid phase separation during casting, which leads to Fe segregation to form coarse spherical and dendritic phases of Fe.^[1-3] After deformation, the Fe phase changes from dendritic or spherical to fibrous, which ultimately leads to an improvement in the mechanical properties of the Cu-Fe

alloy.^[4] The coarse Fe phase is not favorable for the formation of fine Fe fibers, resulting in a weaker Fe-fiber-strengthening effect.^[4,5] In addition, Fe has greater solubility in Cu alloys and has a great influence on the conductivity of Cu alloys. The conductivity of Cu alloys is significantly reduced by the addition of Fe. Therefore, it is important to suppress the segregation and promote the precipitation of the Fe phase to obtain high-performance Cu-Fe alloys.

It has been reported that adding Ag^[6,7] to Cu-Fe alloys can significantly improve their mechanical properties and conductivity. Gao^[8] and Li^[9] have demonstrated that the tensile strength and conductivity of the Cu-Fe alloy increased by > 66 MPa and 4 pct IACS, respectively, after the addition of Ag. They attributed this effect to Ag inhibiting Fe segregation and promoting the precipitation of the Fe phase. Microalloying elements such as Cr,^[10] Si,^[11,12] and Nb^[1] can also improve the mechanical properties; however, they do not improve conductivity. One of the studies carried out by Kim^[10] demonstrated that the addition of Cr can significantly improve the tensile strength and softening performance of Cu-Fe alloys. Furthermore, previous studies have also shown that casting methods such as double-melt mixed casting,^[5] casting under a magnetic field,^[13,14] directional solidification,^[15,16] and upward

DAWEI YUAN and JINSHUI CHEN are with the Faculty of Materials Metallurgy and Chemistry, JiangXi University of Science and Technology, Ganzhou, 341000 P.R. China. XIANGPENG XIAO, HAO HUANG, BAIXIONG LIU, and BIN YANG are with the Faculty of Materials Metallurgy and Chemistry, JiangXi University of Science and Technology and also with the JiangXi Advanced Copper Industry Research Institute, Yingtan, 335000 P.R. China. Contact e-mail: xiao_xiangpeng@126.com; yangbin@jxust.edu.cn BAOJUN HAN is with the School of Chemistry and Chemical Engineering, Gannan Normal University, Ganzhou, 341000 P.R. China.

Manuscript submitted October 19, 2020, accepted March 7, 2021.

Article published online April 8, 2021

continuous casting^[17] can significantly optimize the structure of Cu and Cu-Fe alloys. Wang^[5] obtained a Cu-10Fe alloy casting billet with a uniform Fe phase distribution by double-melt mixed casting. The Fe phase aligned with an external magnetic field, effectively improving the distribution of Fe and inhibiting its segregation.^[13] Directional solidification casting has a bottom-up thermal field and carries a certain induction magnetic field, which can improve the distribution of alloying elements. The grains of the Cu-Cr-Ag alloy prepared by upward continuous casting are columnar and arranged upward, resulting in high strength, high conductivity, and good elongation of the Cu-Cr-Ag alloy.^[18] The effect of the magnetic field on the birth phase of Al-12Si-11.8Mg-6.5Ti was studied by Hao,^[19] who confirmed that a uniform magnetic field could improve the homogeneity of the primary Mg₂Si because of the Lorenz and magnetic forces. The primary (Al,Si)₃Ti phase is distributed along the direction of the magnetic field. A patent by Lu^[20] stated that during the solidification stage, the AC magnetic field can effectively refine Fe dendrites and reduce Fe segregation. Directional solidification results in a large temperature gradient and a certain self-induced magnetic field, which can effectively optimize the alloy structure. However, there are few reports on the effect of directional solidification on the Fe phase morphology, mechanical properties, and electrical conductivity of Cu-Fe-Cr-Ag alloys with a high Fe content.

The present study was conducted to investigate the effect of directional solidification (DS) and upward continuous casting (UCC) on the microstructure and properties of Cu-Fe-Cr-Ag. The purpose of this study was to further optimize the morphology and distribution of Fe and Ag in the Cu-Fe-Cr-Ag alloy and to provide a theoretical guidance for advancements in the Cu-Fe alloy casting technology.

II. EXPERIMENTAL METHOD

Copper (99.99 wt pct), silver (99.99 wt pct), iron (99.95 wt pct), and Cu-8 wt pct Cr master alloy were used as raw materials and melted in a medium frequency induction furnace. Furthermore, Cu-6.5Fe-0.2Cr-1Ag rods with a diameter of 12 mm were prepared by directional solidification (DS) and upward continuous (UCC) casting. The melt temperature is 1250 °C to 1300 °C, and pulling-down speed is 1 mm/s during directional solidification. The melt temperature is 1250 °C to 1300 °C during upward continuous casting, and the traction speed, pitch, and dwell time are 10 mm/s, 4 mm, and 0.41 s, respectively. The composition of the rod was determined using inductively coupled plasma emission spectroscopy (ICP; IRIS Intrepid II, Thermo Fisher Scientific); the results are shown in Table I.

Two Cu-Fe-Cr-Ag alloy rods were prepared using the following process: (1) Homogenization at 950 °C for 2 h, cooling with furnace. (2) Cold drawing with accumulated strain of $\eta = 3.7$ (where $\eta = \ln(A_0/A_d)$, A_0 and A_d are the original and drawn cross-sections, respectively); (3) annealing at 500 °C for 1 h; (4) cold drawing with

Table I. Chemical Compositions of the Upward Continuous Casting Samples (Wt Pct)

	Sample	Fe	Cr	Ag	Cu
DS	Cu-6.5Fe-0.2Cr-1Ag	6.6	0.2	1	bal.
UCC	Cu-6.5Fe-0.2Cr-1Ag	6.4	0.21	0.9	bal.

accumulated strain of $\eta = 5$; (5) isochronous aging at 250 °C, 300 °C, 350 °C, 400 °C, 450 °C, 500 °C, and 550 °C for 1 h and isothermal aging at 300 °C for 0.5, 1, 2, 4, and 8 hours.

The tensile strength and resistance were measured using a universal testing machine (UTM5105X; Shenzhen Sansi Testing Co., Ltd.) and direct current resistance tester (SB-2230; Shanghai Jingmi), respectively. The conductivity (δ) was calculated using formula [1] (where L is the effective length, S is the cross-sectional area, R is the resistance, and K is the temperature coefficient). The microstructures of the samples with different states were observed by optical microscopy (OM; BMM90AE, Shanghai Bimu), scanning electron microscopy (SEM; MLA650F, FEI), and transmission electron microscopy (TEM; TecnaiG2-20, FEI). The voltages of the TEM and SEM were 200 and 20 kV, respectively. OM and SEM samples were prepared by grinding and polishing; they were then corroded with a mixed aqueous solution of 80 mL H₂O + 20 mL HNO₃. The samples were initially ground to a thickness of approximately 50 μ m with 600 to 2000 mesh SiC paper and then punched into a disc with a diameter of 3 mm. Finally, the samples were subjected to electrolytic double spraying at 238 K. The double spraying liquid was a mixture of HNO₃ and C₂H₅OH at a ratio of 3:7. To assess the phase structure, dislocation density, and lattice parameters, powder X-ray diffraction (XRD) was performed using an Xpert Powder diffractometer (PANalytical B.V.) with Cu K α radiation at 40 kV and 40 mA. The XRD samples were sequentially ground using 600 to 2000 mesh SiC paper and electropolished with a mixed aqueous solution of 70 mL H₂O + 30 mL H₃PO₄ to remove the effect of grinding stress on lattice parameters.

$$\delta = \frac{0.01724L}{SRK} \quad [1]$$

III. RESULTS

A. Microstructure Analysis

1. As-cast microstructure analysis

The photomicrographs of the cross sections and vertical sections of the as-cast Cu-Fe-Cr-Ag alloy were prepared by directional solidification and upward continuous casting, as shown in Figure 1. Coarse spherical and dendritic Fe phases were observed in the upward continuously casted Cu-Fe-Cr-Ag alloy (Figures 1(a) and (b)). In multiple casting tests of the directionally

solidified Cu-Fe-Cr-Ag alloy, it was found that the fine dendritic Fe phases arranged along the direction of directional solidification (Figures 1(d) and (e)). Furthermore, fine Fe particles were distributed uniformly along the grain boundaries. It was worth noting that the second phase (thickness of 300 μm) was evenly distributed on the grain boundary surrounding the edge of the directionally solidified Cu-Fe-Cr-Ag alloy, while such features were not observed in the upward continuously casted Cu-Fe-Cr-Ag alloy (Figures 1(c) and (f)).

Figure 2 shows SEM images of the as-cast Cu-Fe-Cr-Ag alloy prepared by directional solidification and upward continuous casting. It can be observed that the Fe dendrites and Fe-rich spheres correspond with the results presented in Figure 1. The directionally solidified Cu-Fe-Cr-Ag alloy contained a second phase distributed at the grain boundaries, mainly outside the cast rod from Figure 2(c). Figure 3 shows the EDS mapping

result of the as-cast Cu-Fe-Cr-Ag alloy prepared by directional solidification. Based on these results, the second phase distributed at the grain boundary was identified as Ag (Figure 3(d)), indicating that Cu and Ag form a Cu-Ag eutectic structure. In addition, the Cr phase mainly dissolved in the Fe phase (Figures 3(b) and (c)).

2. Microstructure evolution of Cu-Fe-Cr-Ag during deformation heat treatment

Figure 4 shows OM images of directionally solidified Cu-Fe-Cr-Ag and upward continuously casted Cu-Fe-Cr-Ag alloy after cold drawing at $\eta = 5$ and aging at 300 $^{\circ}\text{C}$ and 450 $^{\circ}\text{C}$ for 1 h. After cold drawing at $\eta = 5$, the Fe dendrites transformed into Fe fibers (Figures 4(a) and (d)). However, the spherical Fe phase still existed in the upward continuously casted Cu-Fe-Cr-Ag alloy, indicating that it is more difficult for the coarse spherical

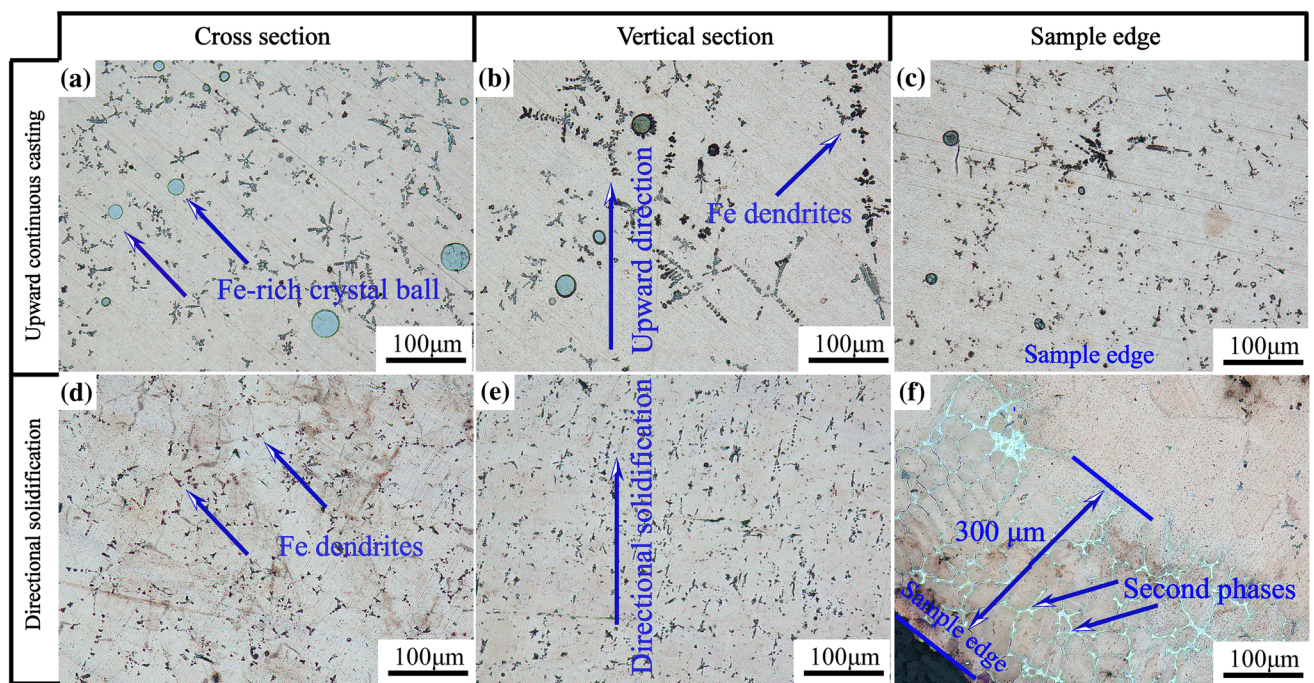


Fig. 1—OM organization of as-cast Cu-Fe-Cr-Ag. (a), (b), (c) Upward continuous casting; (d), (e), (f) directional solidification; (a), (d) cross section; (b), (e) vertical section; (c), (f) sample edge.

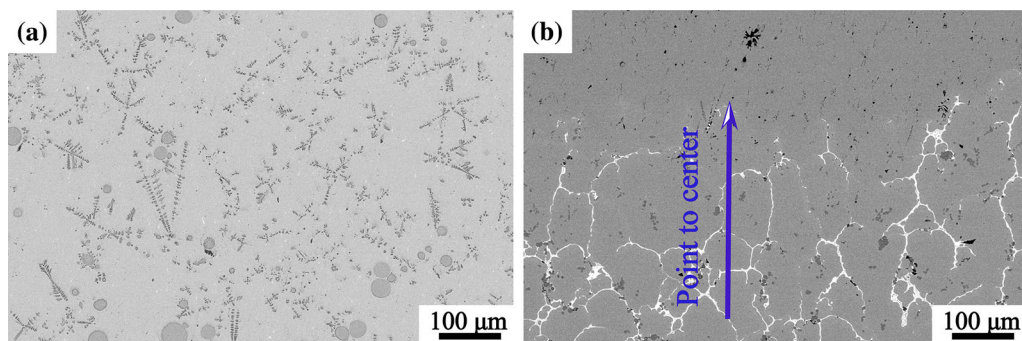


Fig. 2—SEM organization of as-cast Cu-Fe-Cr-Ag alloy cross section. (a) Upward continuous casting; (b) directional solidification.

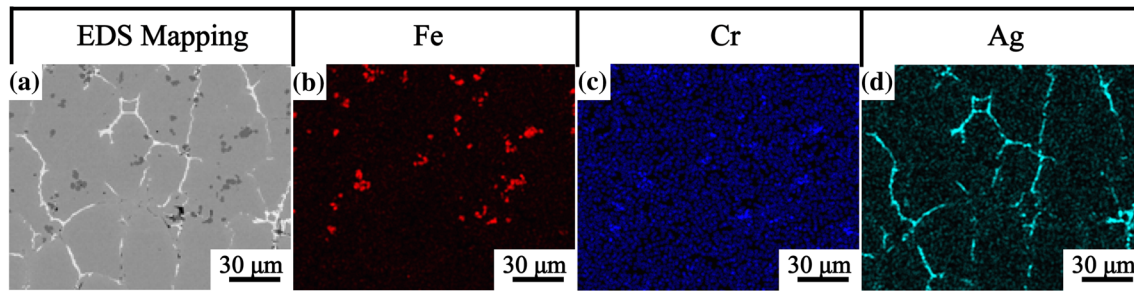


Fig. 3—EDS mapping result of as-cast Cu-Fe-Cr-Ag alloy by directional solidification. (a) EDS face scan location map; (b) Fe; (c) Cr; (d) Ag.

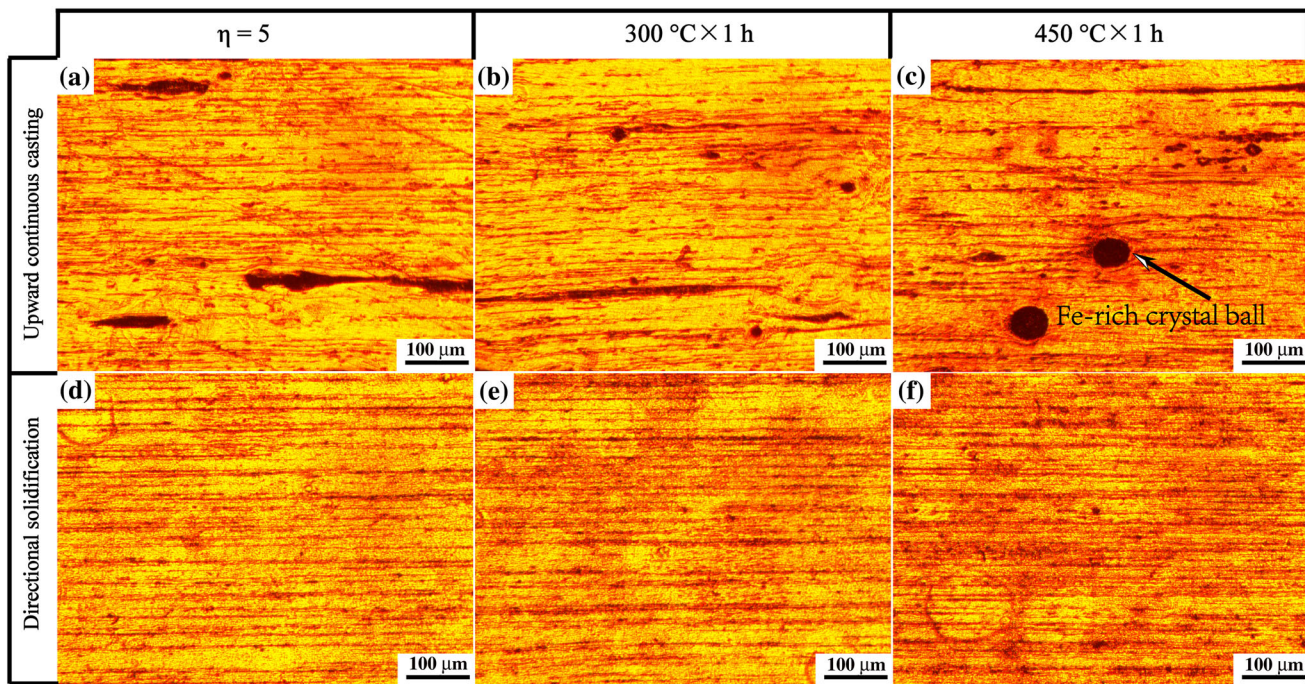


Fig. 4—OM organization of Cu-Fe-Cr-Ag alloy after cold drawing at $\eta = 5$ and aging at 300 °C and 450 °C for 1 h. (a), (b), (c) Upward continuous casting; (d), (e), (f) directional solidification.

Fe phase to form fibers (Figures 4(a) and (c)). Compared with the upward continuously casted Cu-Fe-Cr-Ag, the Fe fibers in the directionally solidified Cu-Fe-Cr-Ag alloy were distributed more uniformly and densely (Figures 4(d) and (e)). Furthermore, there was no evident change after aging at 300 °C and 450 °C for 1 h (Figures 4(b), (c) and (e), (f)).

To further determine the evolution law of Fe fibers during aging, the SEM structure of directionally solidified and upward continuously casted Cu-Fe-Cr-Ag alloy was examined, as shown in Figure 5. After cold drawing at $\eta = 5$ and aging at 300 °C for 1 h, the morphology of the Fe fibers was consistent with that of the OM structure. The Fe fibers coarsened and spheroidized with increasing aging temperature (Figures 5(c), (d), (g), and (h)). Moreover, previous reports have demonstrated that fine Fe fibers are more prone to coarsening and spheroidization during aging.^[21] Therefore, the Fe fibers in the directionally

solidified Cu-Fe-Cr-Ag alloy preferentially spheroidized at 550 °C.

Figure 6 shows the EDS mapping result of directional solidification of Cu-Fe-Cr-Ag and upward continuously casted Cu-Fe-Cr-Ag alloy after cold drawing at $\eta = 5$ and aging at 450 °C for 1 h. It can be observed that Ag is uniformly distributed in the upward continuously casted Cu-Fe-Cr-Ag alloy (Figures 6(b), (f), and (j)). However, a large amount of Ag is distributed on the edge (0 to 500 nm) of the directionally solidified Cu-Fe-Cr-Ag alloy. Moreover, nanoscale Ag particles also precipitated inside the sample, as shown in Figure 6(e). However, after peeling (i.e., the removal of the 300-mm-thick Cu-Ag eutectic structure from the surface layer of the as-cast alloy by grinding) of the directionally solidified Cu-Fe-Cr-Ag, there was no Ag phase distribution at the edge of the sample (Figure 6(i)).

Figure 7 shows TEM images of the directionally solidified Cu-Fe-Cr-Ag and upward continuously casted

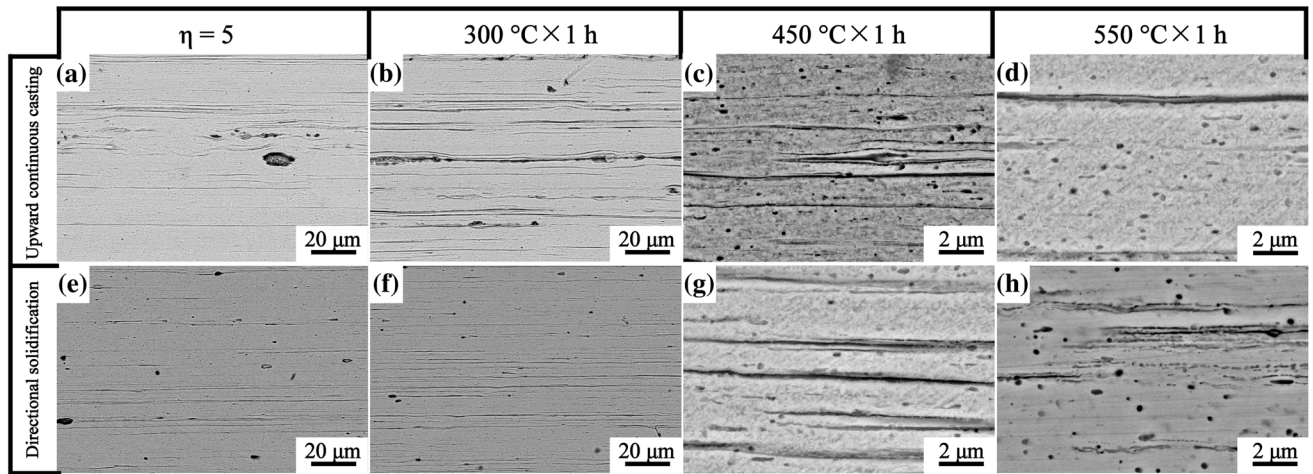


Fig. 5—SEM organization of Cu-Fe-Cr-Ag alloy after cold drawing at $\eta = 5$ and aging at 300 °C, 450 °C, and 550 °C for 1 h. (a), (b), (c), (d) Upward continuous casting; (e), (f), (g), (h) directional solidification.

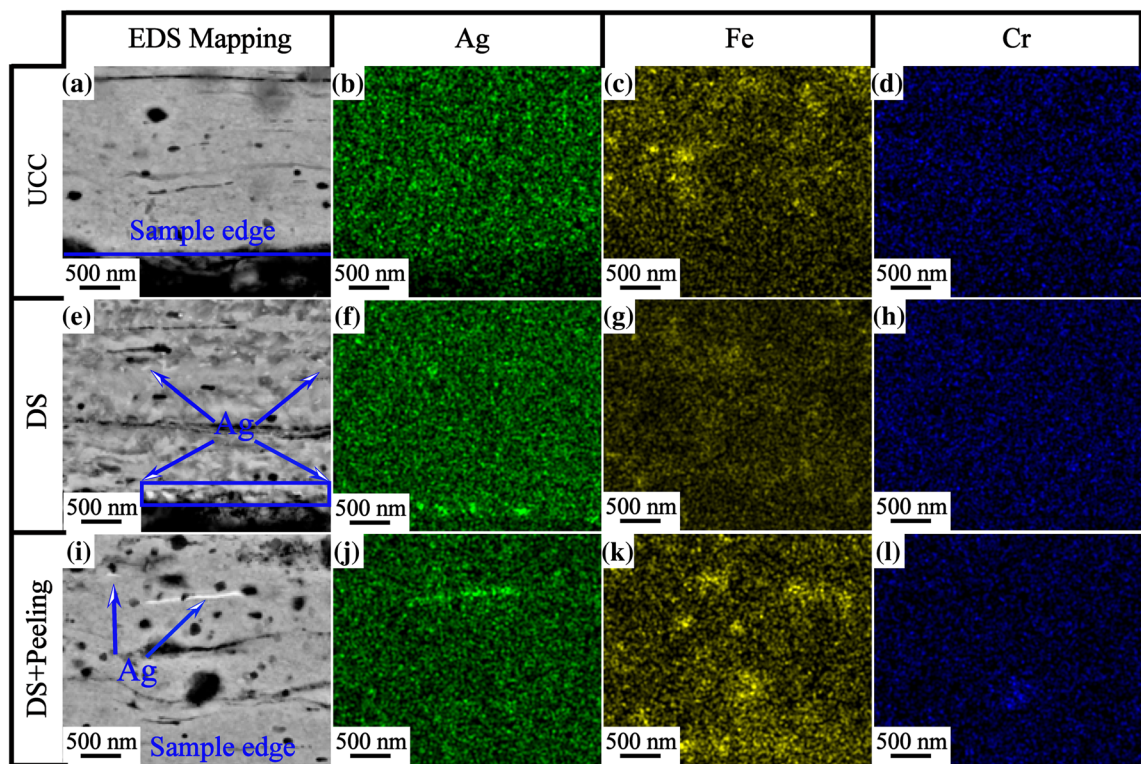


Fig. 6—EDS mapping result of directionally solidified Cu-Fe-Cr-Ag and upward continuously casted Cu-Fe-Cr-Ag alloy after cold drawing at $\eta = 5$ and aging at 450 °C for 1 h. (a), (b), (c), (d) Upward continuous casting (UCC); (e), (f), (g), (h) directional solidification (DS); (i), (j), (k), (l) directional solidification (DS) + peeling.

Cu-Fe-Cr-Ag alloy after cold drawing at $\eta = 5$ and aging at 450 °C for 1 h. After cold drawing, the elongated Cu grains and fibrous Fe phases were distributed in the two alloys. Furthermore, the thicknesses of the Cu grains and Fe fibers in the directionally solidified Cu-Fe-Cr-Ag alloy were smaller (Figures 7(a), (d), and (g)). There was no significant difference in the directionally solidified Cu-Fe-Cr-Ag before and after peeling. The EDS results are shown in Table II. According to Figures 7(d), (g) and Table II, the Ag

phase particles were distributed near the grain boundaries in the directionally solidified Cu-Fe-Cr-Ag. After aging at 450 °C for 1 h, many nano-Fe precipitates and striped Fe phases appeared in the copper matrix (Figures 7(b), (h), and (e)), where the striped Fe phase was the discontinuous phase at the Cu grain boundary. The precipitates and strip-shaped Fe phases in the directionally solidified Cu-Fe-Cr-Ag alloy were finer. Furthermore, Figures 7(c), (f), and (i) shows that the Fe phase was mainly $[001]_{\alpha\text{-Fe}}$ with a bcc structure, and the

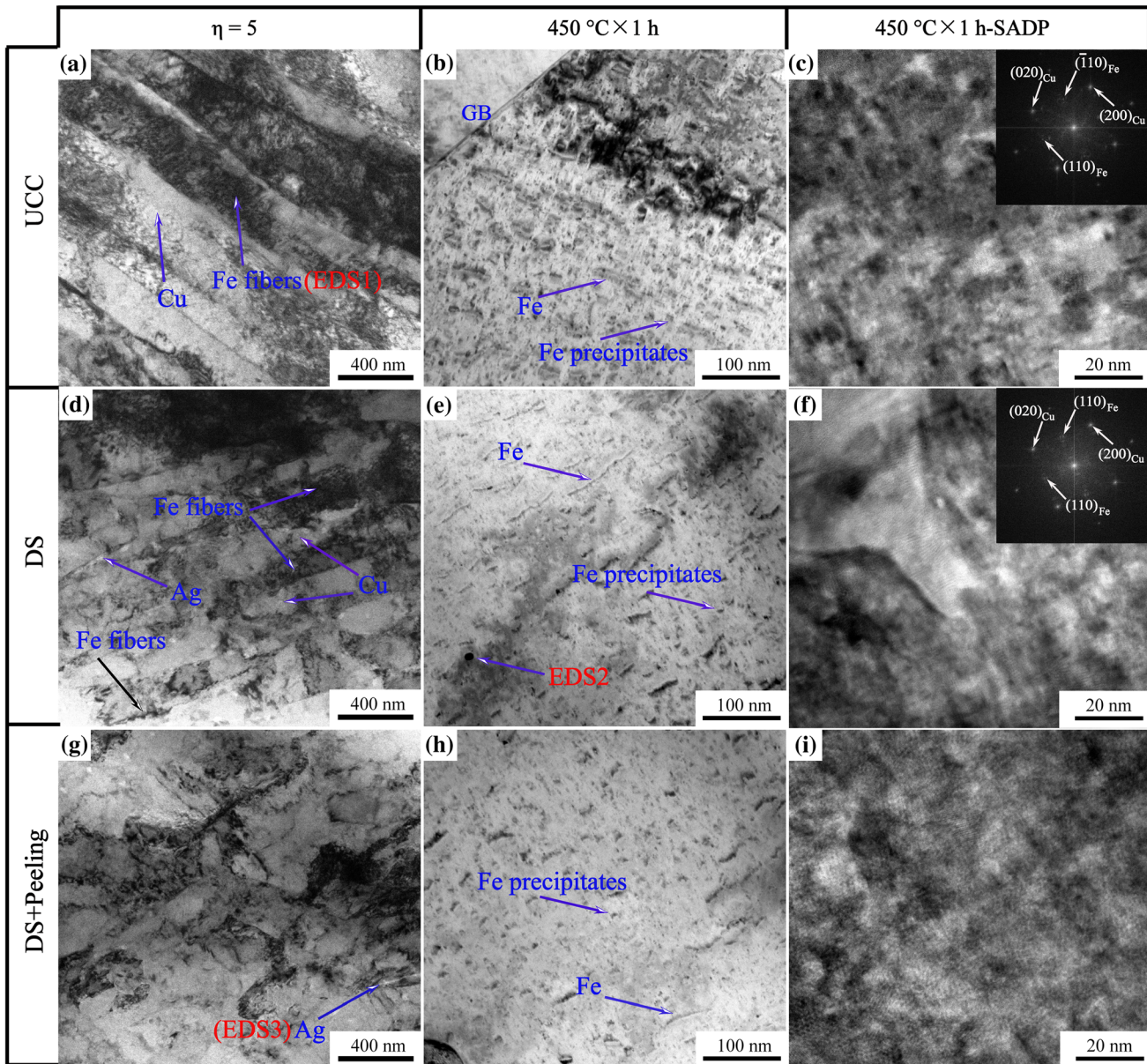


Fig. 7—TEM organization of directionally solidified Cu-Fe-Cr-Ag and upward continuously casted Cu-Fe-Cr-Ag alloy after cold drawing at $\eta = 5$ and aging at 450 °C for 1 h. (a), (b), (c) Upward continuous casting (UCC); (d), (e), (f) directional solidification (DS); (g), (h), (i) directional solidification (DS) + peeling.

Table II. Results of the Quantities in EDS Analysis of Fig. 8(b), (g) and (h)

Element (Wt Pct)	Cu	Fe	Cr	Ag
EDS1	25.84	68	5.28	0.88
EDS2	77	21.9	0.8	0.3
EDS3	96.5	1.11	0.11	2.28

Fe precipitates and Cu matrix had a $(110)_{\alpha\text{-Fe}} // (\bar{2}20)_{\text{Cu}}$ phase relationship.

Figure 8 shows the XRD patterns for the directionally solidified Cu-Fe-Cr-Ag and upward continuously

casted Cu-Fe-Cr-Ag alloy after cold drawing at $\eta = 5$ and aging at 450 °C for 1 h. Figure 8 shows that Cu and Fe peaks are present, and Fe mainly exists in the Cu matrix as $(110)_{\alpha\text{-Fe}}$, $(200)_{\alpha\text{-Fe}}$, and $(211)_{\alpha\text{-Fe}}$. To explore the degree of distortion of Cu-Fe-Cr-Ag under different conditions, the lattice constants of the two alloys were calculated, and the results are shown in Table III. Noticeably, the lattice constant of the directionally solidified Cu-Fe-Cr-Ag alloy was smaller than that of the upward continuously casted alloy, which proves that the latter alloy had a greater degree of lattice distortion. After aging at 450 °C for 1 h, the lattice constants of the two alloys decreased, indicating that the degree of lattice distortion of Cu-Fe-Cr-Ag was alleviated.

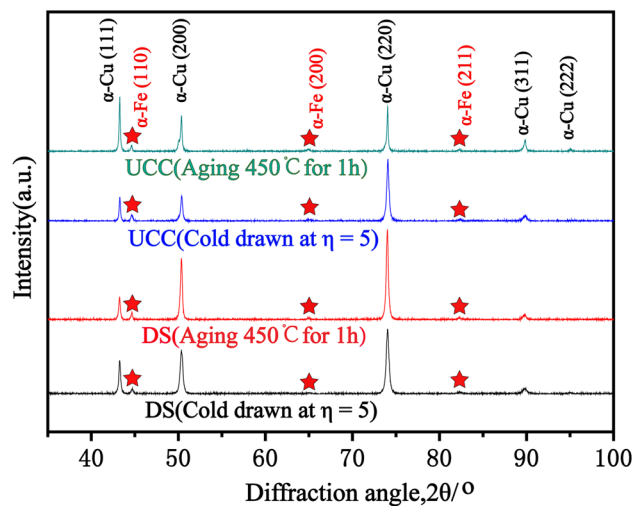


Fig. 8—XRD patterns of directionally solidified Cu-Fe-Cr-Ag and upward continuously casted Cu-Fe-Cr-Ag alloy after cold drawing at $\eta = 5$ and aging at 450 °C for 1 h. (DS, directional solidification; UCC, upward continuous casting).

Table III. Lattice Constant of Cu After Cold Drawing at $\eta = 5$ and Aging at 450 °C for 1 h

Sample	Lattice Constant/nm	
	Prior to Aging	After Aging
UCC	$0.361774 \pm 9.3 \times 10^{-6}$	$0.361687 \pm 2.8 \times 10^{-6}$
DS	$0.361746 \pm 2.03 \times 10^{-6}$	$0.361642 \pm 5.8 \times 10^{-6}$
Δ	2.8×10^{-5}	4.5×10^{-5}

B. Performance Analysis

1. Tensile strength

Figure 9 shows the tensile strength of as-cast Cu-Fe-Cr-Ag prepared by directional solidification and upward continuous casting. The tensile strength of the two alloys is essentially the same, with values > 310 MPa.

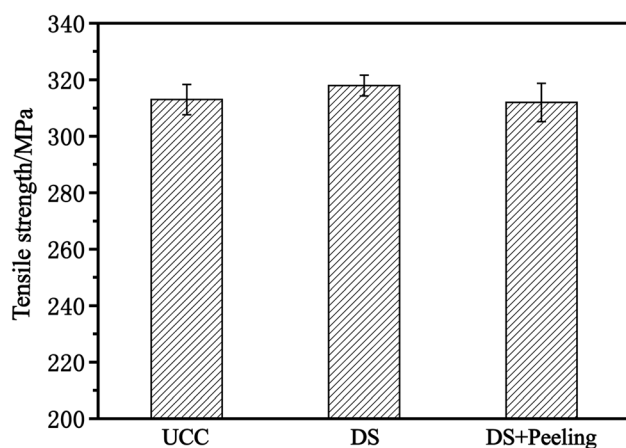


Fig. 9—Tensile strength of as-cast Cu-Fe-Cr-Ag alloy. (DS, directional solidification; UCC, upward continuous casting).

After peeling, the tensile strength of the directionally solidified Cu-Fe-Cr-Ag alloy decreased slightly.

Figure 10 shows the tensile strength of the directionally solidified Cu-Fe-Cr-Ag and upward continuously casted Cu-Fe-Cr-Ag alloys after isochronal aging for 1 h and isothermal aging at 300 °C. Initially, the tensile strength of the alloys increased upon aging; then, it showed a decreasing trend with increasing aging temperature due to the softening of the alloys. The peak tensile strength of the directionally solidified Cu-Fe-Cr-Ag was 789 MPa, which was 21 MPa higher than that of the upward continuously casted Cu-Fe-Cr-Ag. However, the tensile strength of the latter was higher when the aging temperature was > 400 °C. The tensile strength after isothermal aging exhibited the same changes as the isochronous tensile strength. The tensile strength reached its peak after aging at 300 °C for 1 h and decreased with increasing aging time.

2. Electrical conductivity

Figure 11 shows the conductivity of as-cast Cu-Fe-Cr-Ag prepared by directional solidification and upward continuous casting. The conductivity of the directionally solidified Cu-Fe-Cr-Ag alloy was higher than that of the upward continuously casted Cu-Fe-Cr-Ag alloy by 2.2 pct IACS. After peeling, the conductivity of the directionally solidified Cu-Fe-Cr-Ag alloy slightly decreased; however, it was still higher than that of the upward continuously casted Cu-Fe-Cr-Ag alloy.

Figure 12 shows the conductivity of the directionally solidified Cu-Fe-Cr-Ag and upward continuously casted Cu-Fe-Cr-Ag alloy after isochronal heat treatment for 1 h and isothermal heat treatment at 300 °C. During aging, the precipitation of the second phase led to a rapid increase in the conductivity of the material. The conductivity of the two alloys reached a peak at 450 °C for 1 h (Figure 12(a)). The conductivity of the alloy decreased as the aging temperature exceeded 450 °C. However, during the low-temperature aging process, the conductivity of both alloys showed increasing trends with increasing aging time (Figure 12(b)). Therefore, the choice of aging temperature is particularly important to improve the conductivity. In addition, the peak conductivity of the directionally solidified Cu-Fe-Cr-Ag alloy reached 65.5 pct IACS, which was 4.7 pct IACS higher than that of the upward continuously casted Cu-Fe-Cr-Ag alloy. As depicted in Figure 12(a), the blue line represents the conductivity of the directionally solidified Cu-Fe-Cr-Ag alloy after peeling, which was between the conductivity of the two alloys.

IV. DISCUSSION

The Cu-6.5Fe-0.2Cr-1Ag rod was prepared by directional solidification and upward continuous casting. The effect of the two preparation processes on the microstructure and properties of the Cu-Fe-Cr-Ag alloy is described in detail, with a focus on the evolution of the second phase and the properties of the two alloys.

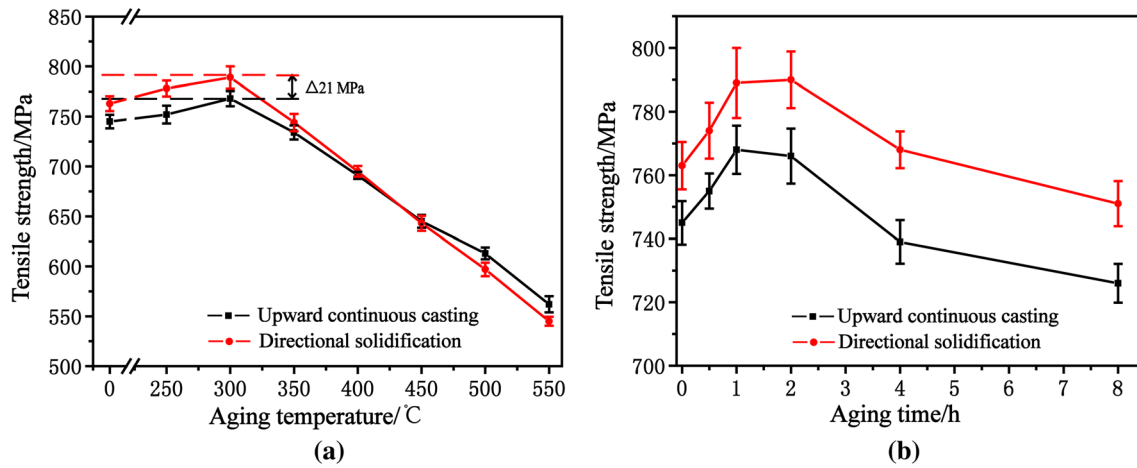


Fig. 10—The tensile strength of as-cast Cu-Fe-Cr-Ag alloy after drawing at $\eta = 5$ and aging. (a) Isochronal heat treatment for 1 h; (b) isothermal heat treatment at 300 °C.

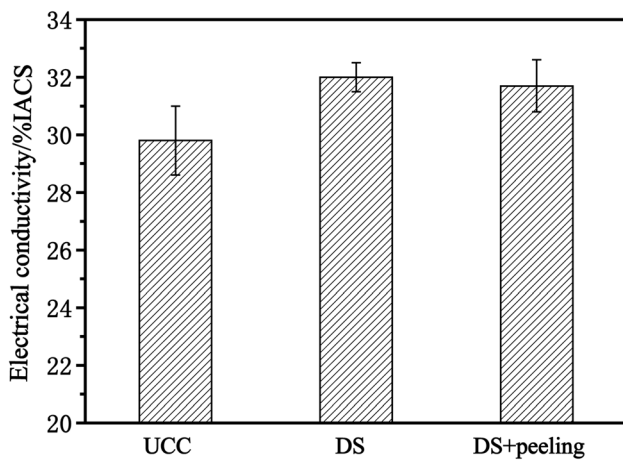


Fig. 11—The conductivity of as-cast Cu-Fe-Cr-Ag. (DS, directional solidification; UCC, upward continuous casting).

A. Evolution of the Fe Phase and Ag Phase in Directionally Solidified Cu-Fe-Cr-Ag Alloy

A schematic diagram of the directionally solidified structure is shown in Figure 13(a); it is composed of ceramic tubes, magnetic induction coils, gallium indium alloy liquid, and cooling circulating water. During directional solidification, the magnetic induction coil can generate a larger magnetic field, which exerts a positive effect on the structure of the alloy. Liu [19] discovered that the primary striped $(Al, Si)_3Ti$ phase was arranged along the direction of the magnetic field. Compared with Cr-, Ag-, Mg-, Al-, and Si-rich particles, Fe-rich particles are more significantly affected by the magnetic field. During the solidification process, Fe particles are subjected to viscous resistance (F_η), buoyancy (F_v), gravity (G), inter-particle force (F_i), and magnetic force (F_M) under the action of a magnetic field. [22] The direction of the magnetic force is identical to that of the magnetic field (Figure 13(b)). Therefore, Fe-rich particles migrate up and down along the

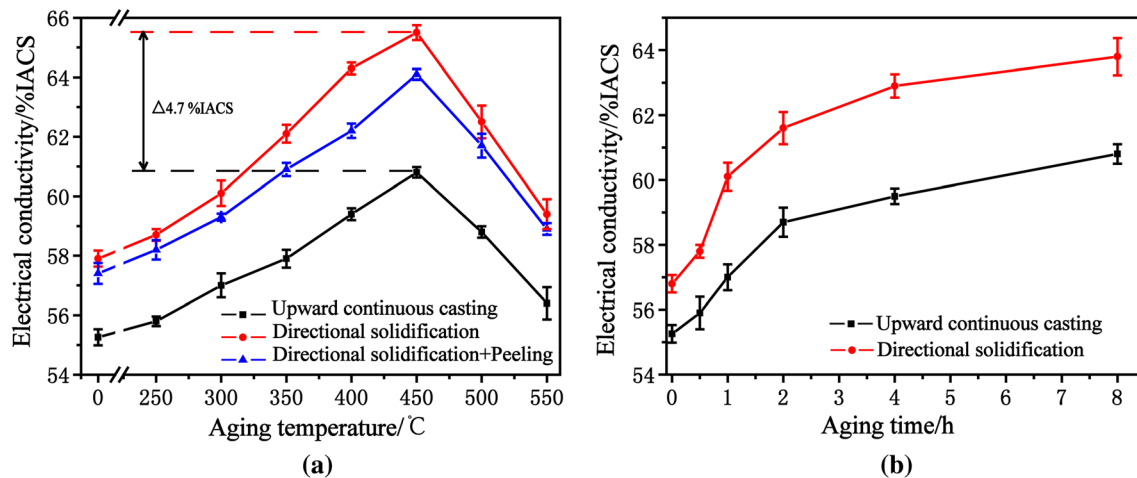


Fig. 12—Conductivity of Cu-Fe-Cr-Ag alloy after drawing at $\eta = 5$ and aging. (a) Isochronal heat treatment for 1 h and (b) isothermal heat treatment at 300 °C.

direction of the applied magnetic field. In addition, the system has the lowest energy in the direction of the magnetic field.^[22] Therefore, the Fe dendrites align with the magnetic field.

In this work, Cu-6.5Fe-0.2Cr-1Ag alloy ingots were prepared by directional solidification and upward continuous casting. The casting method for directional solidification was similar to that of upward continuous casting; the only difference is that directional solidification possesses a large, self-induced magnetic field. Therefore, the Fe dendrites in the Cu-6.5Fe-0.2Cr-1Ag alloy were smaller and arranged along the direction of the induced magnetic field (Figures 1 and 2). Figure 14 shows the solidification process for the directionally solidified Cu-Fe-Cr-Ag alloy. Compared with Cu and Ag, Fe has a higher melting point. Therefore, in the early stage of solidification, Fe nuclei are preferentially formed (Figure 14(a)). The Fe atom core moves up and down and absorbs Fe and Cr in the surrounding melt under an applied magnetic field. According to the

principle of minimum system energy solidification, Fe dendrites arranged in the direction of the magnetic field were finally formed (Figure 14(b)). The Cu-rich liquid phase slowly nucleates with decreasing temperature, which has also been observed in advanced research.^[5] Generally, when the Ag content is only 1 wt pct, the alloy should not have a eutectic composition. However, a degraded eutectic phase was observed in the directionally solidified Cu-Fe-Cr-Ag alloy because of unbalanced solidification (Figures 1(f) and 2(c)). The part closest to the ceramic tube has a higher degree of subcooling during the solidification process. The increasing in the degree of undercooling causes the Cu-Ag eutectic line to move to the left, resulting in a Cu alloy with a low Ag content, which is more likely to form a eutectic structure. Meanwhile, the magnetic field increases the presence of supersaturated Ag in the eutectic Cu and reduces the solubility of solid Ag in the Cu matrix.^[16] In addition, the pre-crystallized Fe phase increases the heterogeneous nucleation of Cu alloys. Therefore, Cu and Ag formed a Cu-Ag eutectic structure at the edge of the alloy rod (Figures 14(c) and (d)).

Furthermore, two Cu-Fe-Cr-Ag alloy rods were prepared using the following process: homogenization at 950 °C for 2 h → cold drawing with an accumulated strain of $\eta = 3.7$ → annealing at 500 °C for 1 h → cold drawing with an accumulated strain of $\eta = 5$. Fe dendrites and Fe-rich crystal balls transformed into Fe fibers, and Cu grains transformed from equiaxed crystals to fibers (Figures 4 and 5). Cu and Fe fibers were arranged intermittently, and their widths in the directionally solidified Cu-Fe-Cr-Ag alloy were smaller because of the finer primary Cu grains and Fe dendrites (Figures 1 and 2). Moreover, the fine Fe dendrites significantly improved the cooperative deformation ability between Cu/Fe.

The dislocation density of the two alloys was calculated using the XRD diagram (Figure 8). The dislocation density (ρ) is expressed as follows^[23,24]:

$$\beta \cos \theta = (4 \sin \theta) \varepsilon + K\lambda/D \quad [2]$$

$$\rho = 3.46\varepsilon/(Db) \quad [3]$$

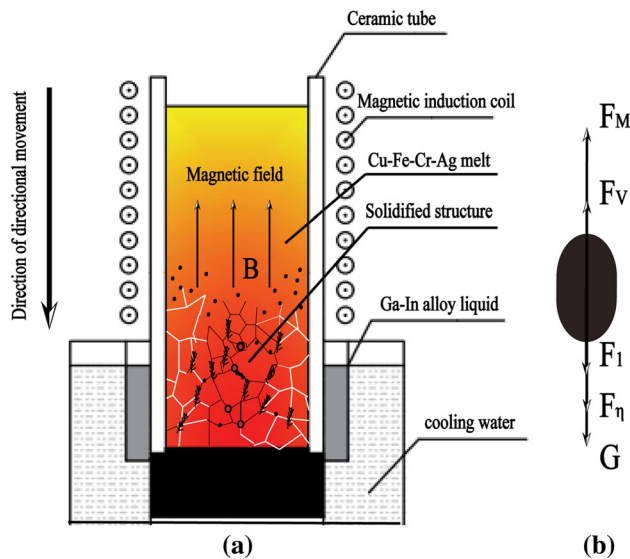


Fig. 13—Schematic diagram of structure during directional solidification (a) and Fe particle force (b).

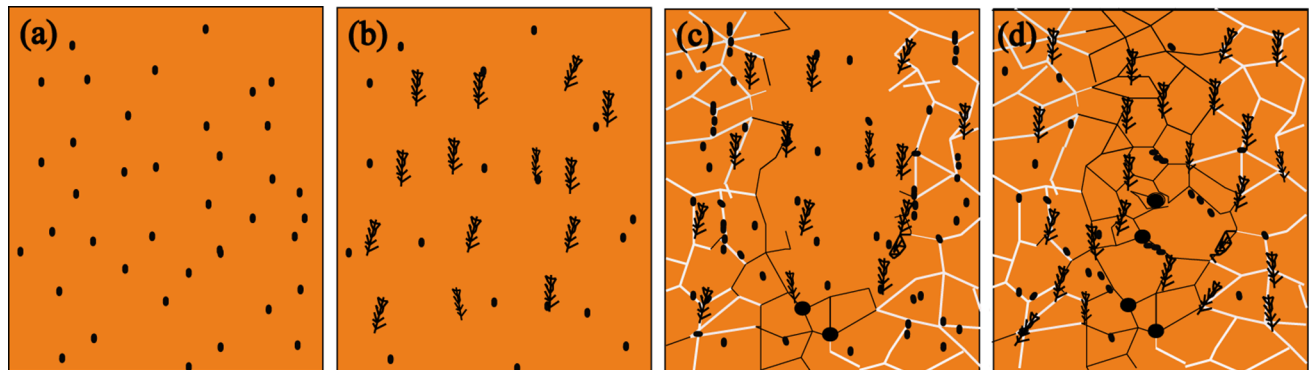


Fig. 14—Schematic view of directionally solidified Cu-Fe-Cr-Ag alloy: (a) early stage of solidification; (b) Fe fiber formation stage; (c) formation stage of Cu-Ag eutectic structure; (d) final organization diagram.

where β is the XRD peak broadening, θ is the diffraction angle, ε is the microstrain, K is a constant (0.9), D is the grain size, λ is the wavelength of Cu K α radiation (0.15405 nm), and b is the magnitude of the Burgers vector. The microstrain (ε) is the slope of the linear fit of the $\beta\cos\theta-4\sin\theta$ plot. Table IV revealed that the dislocation density of the directionally solidified Cu-Fe-Cr-Ag alloy was greater than that of the upward continuously casted Cu-Fe-Cr-Ag alloy. Fine Fe fiber, large fiber spacing, and high dislocation density contributed to the mechanical properties of the alloy.^[4,25] Therefore, the tensile strength of the directionally solidified Cu-Fe-Cr-Ag alloy was higher than that of the upward continuously casted Cu-Fe-Cr-Ag alloy (Figure 10).

B. Analysis of Electrical Conductivity of Directionally Solidified Cu-Fe-Cr-Ag and Upward Continuously Casted Cu-Fe-Cr-Ag alloy

On the basis of Matthiessen's rule, the electrical resistance (ρ_{total}) of the alloy can be expressed^[26-28]:

$$\rho_{\text{total}} = \rho_m + \rho_s + \rho_p + \rho_d \quad [4]$$

where ρ_m represents the resistivity introduced by the Cu matrix, ρ_s represents the resistivity introduced by solute atoms, ρ_p represents the resistivity introduced by nanoscale Fe precipitates, and ρ_d represents the resistivity introduced by lattice defects. Pure Cu has a small resistivity and can be ignored. Compared with the solid-solution atoms, the electron scattering caused by the precipitated particles is much smaller.^[26] Therefore, the resistance caused by the precipitated phase can be ignored. Generally, vacancies and dislocations increase, and grain size decreases as the amount of deformation increases. Vacancies, grain boundary defects, and dislocations can cause lattice distortion to some extent, which can increase the electron scattering rate to a certain extent. Furthermore, the lattice constant of the Cu matrix increases with the increasing of dislocations and grain boundaries. After aging at 450 °C for 1 h, the dislocations and vacancies in the alloy were greatly reduced, and the corresponding electron scattering rate decreased. The effect of Ag and Cr on the conductivity of Cu alloys is also small^[18] and can be ignored. The solid-solution Fe atoms have a significant influence on the Cu alloy. Previous studies have shown that the resistivity will increase by 0.92 $\mu\Omega$ cm for every 0.1 wt pct increase in the Fe content in the Cu matrix.^[29] Therefore, the electron scattering in the Cu-Fe-Cr-Ag alloy is mainly caused by lattice distortion and solid-solution atoms.

Figure 15 shows the relationship between the lattice constant and conductivity of the Cu-Fe-Cr-Ag alloy after cold drawing and after aging at 450 °C for 1 h. The solid-solution content of Fe in the Cu matrix was estimated using Eq. [5]^[30,31]:

$$C = \left| \frac{\alpha - \alpha_1}{\alpha_2 - \alpha_1} \right| \times 100 \text{ pct} \quad [5]$$

Table IV. Dislocation Density of Cu-Fe-Cr-Ag Alloy

Sample	Dislocation Density (m^{-2})	
	Prior to Aging	After Aging
UCC	9.76×10^{14}	7.91×10^{14}
DS	1.07×10^{15}	8.72×10^{14}

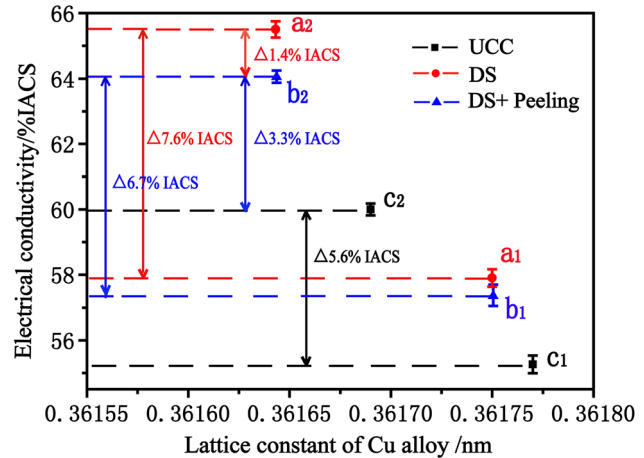


Fig. 15—Correspondence between the lattice constant and conductivity. (a₁, b₁ and c₁: Second cold drawing, a₂, b₂ and c₂: Aging at 450 °C for 1 h. DS, directional solidification; UCC, upward continuous casting).

Table V. Lattice Constant of Cu After Cold Drawing at $\eta = 5$ and Aging at 450 °C for 1 h

Sample	Solubility of Fe/At. Pct	
	Prior to Aging	After Aging
UCC	0.378	0.262
DS	0.34	0.2

where α , α_1 and α_2 are the lattice constants of the solid solution, solvent, and solute, respectively. The calculated results are shown in Table V. The lattice constant of the directionally solidified Cu-Fe-Cr-Ag alloy was smaller than that of the upward continuously casted Cu-Fe-Cr-Ag alloy, which led to higher conductivity of the former. After aging, the nanoscale Fe phase of the two alloys precipitated from the Cu matrix (Figure 7), and the dislocation density was greatly reduced (Table IV). The lattice constants of the two alloys decreased because of the precipitation of the Fe phase and the reduction of dislocation density. The lattice constant of the directionally solidified Cu-Fe-Cr-Ag alloy decreased more significantly, resulting in excellent electrical conductivity of the directionally solidified Cu-Fe-Cr-Ag alloy.

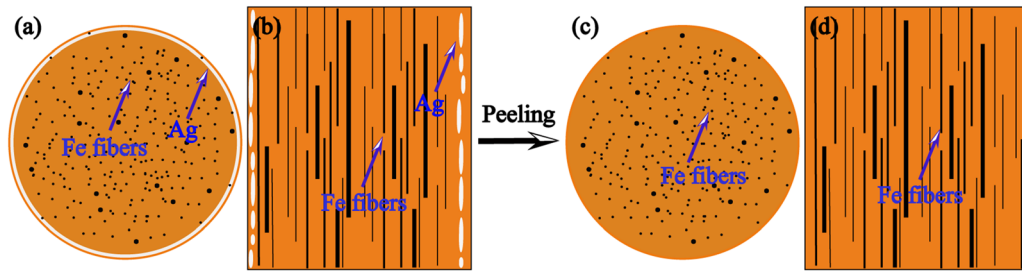


Fig. 16—Schematic diagram of Ag and Fe distribution before and after peeling. (a), (b), (c), (d) directional solidification; (a), (c) cross section; (b), (d) vertical section.

However, it was worth noting that the conductivity of the directionally solidified Cu-Fe-Cr-Ag alloy decreased after peeling (Figure 12(a)). The conductivity of Ag was higher than that of Cu. Before and after peeling, the only difference was in the distribution of Ag around the pattern; Ag was distributed along the edge of the pattern before peeling (Figure 6(e)), and its morphology and structure were similar to those of Ag-clad Cu (Figures 16(a) and (b)). The Ag-clad Cu structure was removed after peeling (Figures 16(c) and (d)), resulting in a decrease in the conductivity of the alloy. Therefore, a structure similar to that of Ag-clad Cu may partially explain the better conductivity of the directionally solidified Cu-Fe-Cr-Ag alloy.

These analyses demonstrate that the higher conductivity of the directionally solidified Cu-Fe-Cr-Ag alloy was due to the small lattice constant, lower solubility of Fe in the Cu matrix, and unique structure similar to that of Ag-clad Cu.

V. CONCLUSIONS

- (1) The Cu-Fe-Cr-Ag alloy prepared by directional solidification contained finer and uniform Fe dendrites distributed along the magnetic field and effectively suppressed the segregation of the Fe phase. In contrast, the Cu-Ag eutectic structure was distributed on the edge of the alloy and formed a structure similar to Ag-clad Cu after cold drawing. In addition, the fine and directional Fe dendrites enhanced the co-denaturation ability of Cu/Fe.
- (2) Compared with the upward continuous casting preparation method, the Cu-Fe-Cr-Ag alloy prepared by directional solidification had a higher tensile strength and conductivity. The peak tensile strength and peak conductivity of directionally solidified Cu-Fe-Cr-Ag reached up to 789 MPa and 65.5 pct IACS, respectively, which were 21 MPa and 4.7 pct IACS higher than those of the upward continuously casted Cu-Fe-Cr-Ag alloy. The higher conductivity of the directionally solidified Cu-Fe-Cr-Ag alloy was attributed to the small lattice constant, lower solubility of Fe in the matrix, and unique structure similar to that of Ag-clad Cu.

ACKNOWLEDGMENTS

This work was supported by the Program of Qingjiang Excellent Young Talents, Jiangxi University of Science and Technology, National Key Research and Development Program of China. (Grant No. 2016YFB0301400), National Natural Science Foundation of China (Grant Nos. 51561008, 51804138, 51761013), and the Program for Excellent Young Talents (JXUST).

REFERENCES

1. P. Zhang, Q. Lei, X.B. Yuan, X.F. Sheng, D. Jiang, Y.P. Li, and Z. Li: *Mater. Today Commun.*, 2020, vol. 25, art. no. 101353.
2. N. Liu: *J. Non-Cryst. Solids*, 2012, vol. 358, pp. 196–99.
3. S.C. Liu, J.C. Jie, B.W. Dong, Z.K. Guo, T.M. Wang, and T.J. Li: *Mater. Des.*, 2018, vol. 156, pp. 71–81.
4. B.D. Sun, H.Y. Gao, J. Wang, and D. Shu: *Mater. Lett.*, 2007, vol. 61, pp. 1002–06.
5. M. Wang, R. Zhang, Z. Xiao, S. Gong, Y.B. Jiang, and Z. Li: *J. Alloys Compd.*, 2020, vol. 820, pp. 1–10.
6. Y.F. Wang, H.Y. Gao, Y.F. Han, Y.B. Dai, J. Wang, and B.D. Sun: *J. Alloys Compd.*, 2017, vol. 691, pp. 992–96.
7. K.M. Liu, D.P. Lu, H.T. Zhou, A. Atrens, J. Zou, Y.L. Yang, and S.M. Zeng: *Mater. Sci. Eng. A*, 2010, vol. 527, pp. 4953–58.
8. H.Y. Gao, J. Wang, D. Shu, and B.D. Sun: *J. Alloys Compd.*, 2007, vol. 438, pp. 268–73.
9. Y. Li, D.Q. Yi, and J.B. Zhang: *J. Alloys Compd.*, 2015, vol. 647, pp. 413–18.
10. D.H. Kim and K.H. Lee: *Korean J. Mater. Res.*, 2010, vol. 20, pp. 60–64.
11. Y.B. Jeong, H.R. Jo, J.T. Kim, S.H. Hong, and K.B. Kim: *J. Alloys Compd.*, 2019, vol. 786, pp. 341–45.
12. S. Sarkar, C. Srivastava, and K. Chattopadhyay: *Mater. Sci. Eng. A*, 2018, vol. 723, pp. 38–47.
13. X.W. Zuo, B.L. An, D.Y. Huang, L. Zhang, and E.G. Wang: *Acta Phys. Sin.*, 2016, vol. 65, art. no. 137401.
14. D.F. Du, Y. Fautrelle, and Z.M. Ren: *Acta Mater.*, 2016, vol. 121, pp. 240–56.
15. Y.Y. Lu, H.X. Zheng, F.Q. Xie, and J.G. Li: *Mater. Sci. Forum.*, 2005, vols. 475–479, pp. 2607–10.
16. X.W. Zuo, R. Guo, C.C. Zhao, L. Zhang, E.G. Wang, and K. Han: *J. Alloys Compd.*, 2016, vol. 676, pp. 46–53.
17. J.Y. Dai, Z.M. Yin, R.R. Jiang, L.P. Song, and Y. Yuan: *Chin. J. of Nonferrous Met.*, 2009, vol. 19, pp. 1840–47.
18. D.W. Yuan, B. Yang, J.S. Chen, H.M. Chen, J.B. Zhang, and H. Wang: *Metall. Mater. Trans. A*, 2017, vol. 48A, pp. 6083–90.
19. T. Liu, Q. Wang, and C.J. Wang: *Metall. Mater. Trans. B*, 2011, vol. 42A, pp. 1863–69.
20. D.P. Lu, L. Lu, Z.B. Lu, J. Zou, K.M. Liu, L. P. Kang, Q.F. Fu, and Z.Z. Wan: *Inst. Appl. Phys. Jiangxi Acad. Sci.*, 2010, CN101775520A.
21. H. Gao, J. Wang, and B. Sun: *J. Alloys Compd.*, 2009, vol. 469, pp. 580–86.

22. X.W. Zuo, B.L. An, D.Y. Huang, L. Zhang, and E.G. Wang: *Acta Phys. Sin.*, 2016, vol. 65, pp. 1–10.
23. H. Cheng, H.Y. Wang, Y.C. Xie, Q.H. Tang, and P.Q. Dai: *Mater. Sci. Technol.*, 2017, vol. 33, pp. 2032–39.
24. Y.H. Zhao, X.Z. Liao, Z. Jin, R.Z. Valiev, and Y.T. Zhu: *Acta Mater.*, 2004, vol. 52, pp. 4589–99.
25. M. Li, H. Wang, Y. Guo, H. Wang, D. Zheng, J. Shan, and Y. Chang: *J. Nucl. Mater.*, 2020, vol. 532, art. no. 152063.
26. H. Gao, J. Wang, D. Shu, and B. Sun: *Scr. Mater.*, 2005, vol. 53, pp. 1105–1107.
27. K. Liu, D. Lu, H. Zhou, Y. Yang, A. Atrens, and J. Zou: *J. Mater. Eng. Perform.*, 2013, vol. 22, pp. 3723–27.
28. S.I. Hong and J.S. Song: *Metall. Mater. Trans. A*, 2001, vol. 32A, pp. 985–90.
29. J.D. Verhoeven, S.C. Chueh, E.D. Gibson: *J. Mater. Sci.*, 1989, pp. 1748–52.
30. J.P. Wu, B. Zhang, and R.L. Wang: *J. Shaanxi Univ.*, 2005, vol. 23, pp. 35–37.
31. Y. Long, W. Wan, G.Y. Qin, N.G. Chen, S. Chen, and Y.T. Ning: *Rare Metal Mater. Eng.*, 2007, vol. 36, pp. 1416–19.

Publisher's Note Springer Nature remains neutral with regard to jurisdictional claims in published maps and institutional affiliations.